

Low-cycle fatigue analysis of a web frame corner in ship structures

Wolfgang Fricke · Nils Friedrich · Luciano Musumeci · Hans Paetzold

Received: 28 October 2013 / Accepted: 30 January 2014 / Published online: 6 March 2014
© International Institute of Welding 2014

Abstract Ship structures are subjected to cyclic loads which may lead to fatigue failures particularly at welded joints. In addition to loads induced by waves and structural vibrations, which contribute to high-cycle fatigue, various structural details are also subjected to a limited number of high-stress cycles caused by changing loading conditions, which may lead to low-cycle fatigue. Thus, appropriate procedures are required for the shipbuilding industry, which are missing in the existing design codes. Experimental investigations and numerical analyses were performed to validate a procedure for the design of ship structures in the low-cycle fatigue regime. Three large-scale fatigue tests were carried out with high bending moments on test models of web frame corners in order to initiate fatigue cracks after few hundred cycles. Different cracks occurred; however, a crack at the cruciform joint has shown to determine the failure of the connection. An extension of the effective notch stress approach was applied to this joint to assess the low-cycle fatigue life, considering the elastic–plastic strain, evaluated by nonlinear finite element analyses, in the notch of the weld toe. This practical method offers promising possibilities to assess the fatigue life of welded joints in the low-cycle fatigue regime.

Keywords Finite element analysis · Low-cycle fatigue · Fatigue tests · Notch effect · Ships · Structures

1 Introduction

Welded ship structures are prone to fatigue as service experience has shown. Most fatigue failures occurred in the high-cycle fatigue (HCF) domain due to wave action, e.g. at side longitudinals. But also fluctuations of still water loads, due to changing loading conditions, contribute to fatigue damage as outlined, e.g. in [1]. These may create rather large elastic–plastic strains in structural details with a relatively low number of load cycles in the order of hundred or thousand load cycles, causing low-cycle fatigue (LCF).

First LCF investigations of ship structural details dealt with free plate edges of cutouts [1] showing the applicability of the cyclic strain approach. The application to welded joints is still limited due to the inhomogeneous geometry and material in the fatigue-critical area [2]. The need for suitable design criteria initiated further investigations [3], resulting in a proposal based on the so-called pseudo-stress. This is the linear-elastic stress which causes an elastic strain of the same amount as the strain in an elastic–plastic analysis. Another proposal is based on the effective notch stress approach commonly applied to HCF using a fictitiously rounded weld toe [4]. It has been shown [5–7] that for different structures with over- and undermatched welded joints, the fatigue lives in HCF and LCF fell into a narrow scatter band if plotted in relation to the effective local strain range.

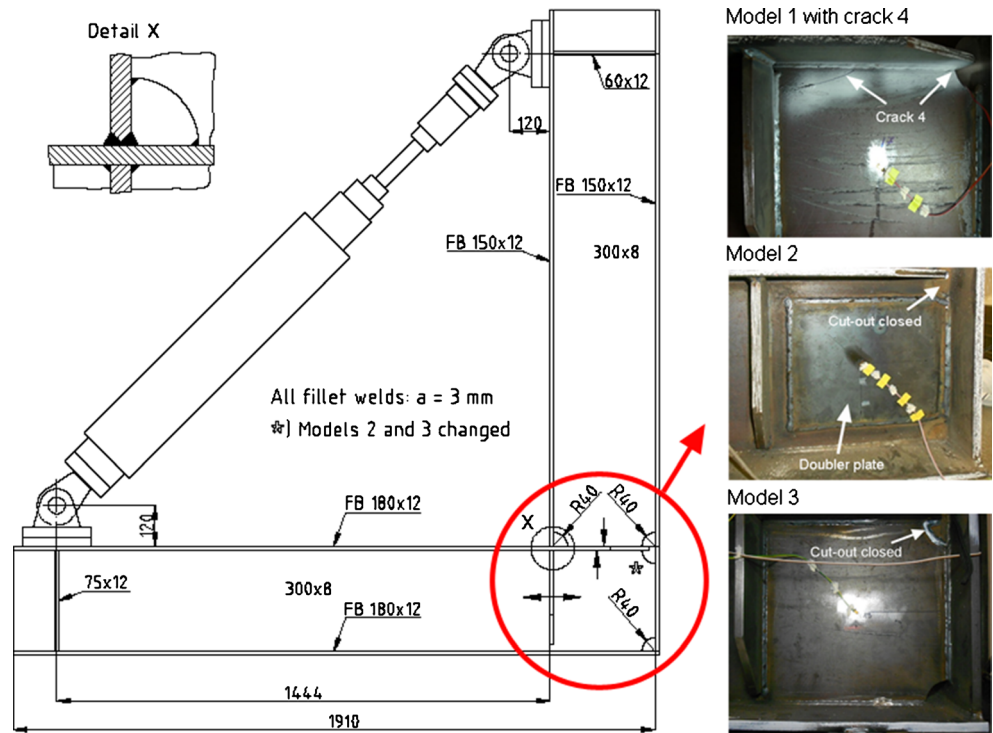
It should be noted that the approaches mentioned may not be suitable for ultra-low-cycle fatigue (ULCF), i.e. crack initiation lives in the order of ten cycles [8, 9].

Doc. IIW-2432, recommended for publication by Commission XIII "Fatigue of Welded Components and Structures"

W. Fricke (✉) · N. Friedrich · H. Paetzold
Institute of Ship Structural Design and Analysis, Hamburg
University of Technology, Hamburg, Germany
e-mail: w.fricke@tu-harburg.de

L. Musumeci
Department of Electronic Engineering, Chemistry & Industrial
Engineering, University of Messina, Messina, Italy

Fig. 1 Web frame corner investigated



Additional experimental and numerical investigations are described in the present paper with the objective to contribute to the development of appropriate procedures for the LCF assessment of welded ship structural details.

2 Structural detail considered

The corner of T-shaped web frames displayed in Fig. 1 has been chosen for the investigation. The frames are built-up T-shaped sections. The structure has been scaled down by a factor of 2 compared to typical ship structures. The loading consists mainly of bending moments created by a 160-kN hydraulic cylinder acting in both directions.

The critical connection is the cruciform joint (detail X) being part of the block joint. Full penetration welding is applied to avoid root cracking. Cutouts are arranged at the cruciform joint and at the right end of the horizontal flange. Mild steel (S235JR) was used for the material, being widely applied in shipbuilding. Welding was performed using the MAG process with a 1.2-mm-thick wire according to DIN ISO 14341-A-G4Si1, having minimum yield strength of 295 MPa.

Three models were fabricated with small modifications. The cutout at the right end of the horizontal flange had to be closed in models 2 and 3 as unexpected crack initiation (4) occurred here in model 1 (see right part of Fig. 1). Model 2 was further reinforced by 4-mm-thick doubler plates on both

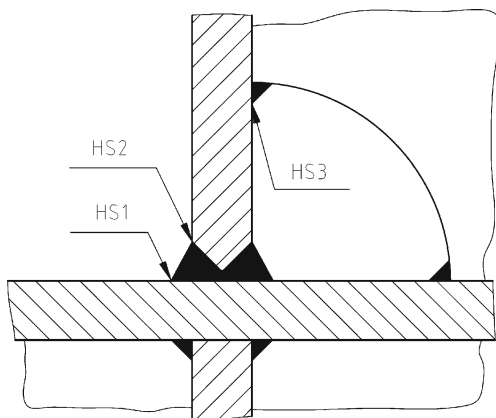


Fig. 2 Definition of hot spots

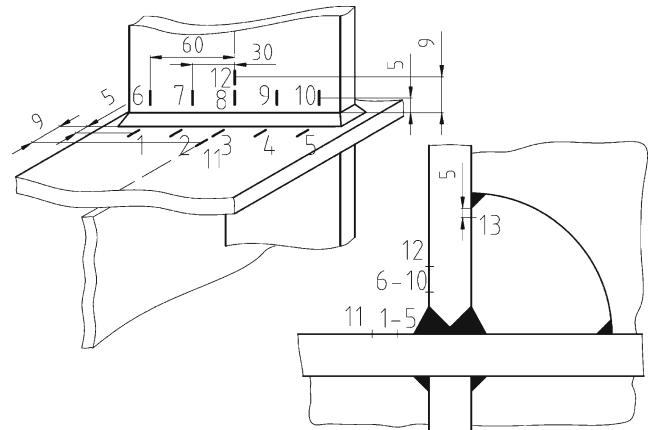


Fig. 3 Arrangement of strain gauges in model 1

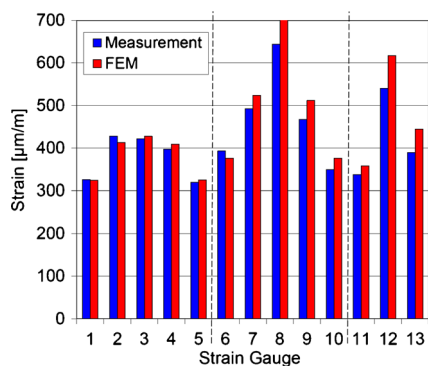


Fig. 4 Comparison between measured and computed elastic strain ($F=25$ kN) in model 1

surfaces of the square web plate in the corner to avoid buckling in view of the high load applied to this model.

3 Elastic stresses at critical hot spots

The three most highly stressed hot spots at weld toes are illustrated in Fig. 2. Hot spot HS2 shows the highest stress resulting finally in the dominant fatigue crack, whereas HS1 is characterized by a sharper weld toe angle and HS3 by a high welding-induced residual stress revealed in a previous study [10]. Strain gauges were arranged at the hot spots as well as along the cruciform joint on both flanges. Further strain gauges were applied for load control in the web frames and on the web plate in the intersection. Figure 3 shows their arrangement for model 1. In addition, finite element analyses were performed for comparison which will be described in Section 5.

The measured and computed strains for model 1 subjected to a force of 25 kN are shown in Fig. 4. The load level is still in the elastic domain. The results agree quite well with each other. An unequal strain distribution along the lower toe (gauges 1–5) and upper toe (gauges 6–10) of the cruciform joint can be observed which is due to the reduced effective

Table 1 Computed structural hot spot stresses σ_{HS} for $F=25$ kN and SCFs

Hot spot	Model 1		Model 2		Model 3	
	σ_{HS} [MPa]	SCF ^a	σ_{HS} [MPa]	SCF ^a	σ_{HS} [MPa]	SCF ^a
HS1	103	2.4	96	2.2	104	2.4
HS2	174	3.5	156	3.1	172	3.4
HS3	138	3.1	138	3.1	137	3.0

^a SCFs refer to the nominal stress at the hot spot location

width of the flange. This effect is expected also in the elastic-plastic domain.

The structural hot spot stresses σ_{HS} were computed on the basis of [4], i.e. for type a hot spots being characterized by weld toe on plate surface. The results are summarized for all three models in Table 1. The highest stress is found at HS2, followed by HS3 and HS1. The differences between the three models are due to the modifications mentioned above. Also given is the stress concentration factor (SCF) based on the nominal stress in the fully effective flange at the respective strain gauge location, i.e. axial force divided by sectional area plus bending moment divided by section modulus for the point considered. The cutout and misalignment effects as well as local plate bending were neglected in the reference stress.

4 LCF tests

The LCF tests were performed at the Hamburg University of Technology (TUHH). Prescribed alternating displacements of the hydraulic cylinder were applied (load ratio $R \approx -1$). The first model was subjected to ± 16.5 mm. Figure 5 shows the development of the upper and lower force, which was almost constant over the first 800 cycles ($+114/-111$ kN), before a drop was observed due to propagating cracks. Model 2 was subjected to ± 16 mm, yielding stabilized forces of $+123/-125$ kN, whereas model 3 was loaded with ± 14.5 mm, yielding stabilized forces of $+111/-101$ kN.

The strain ranges recorded in the models are displayed in Figs. 6, 7 and 8. After starting the tests, the highest strain range was observed in way of HS2, whereas the strain gauge at HS3 showed smaller values and those at HS1 the smallest. Most strain gauges showed pronounced cyclic yielding of the base material

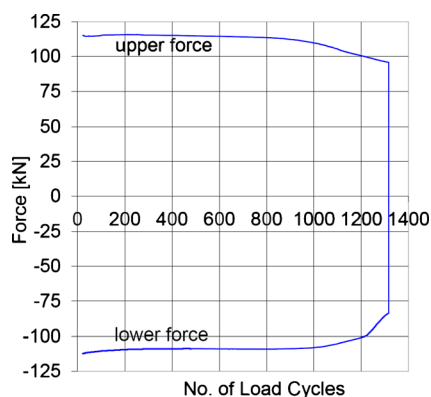


Fig. 5 Force history during LCF test of model 1

Fig. 6 Strain ranges recorded in model 1

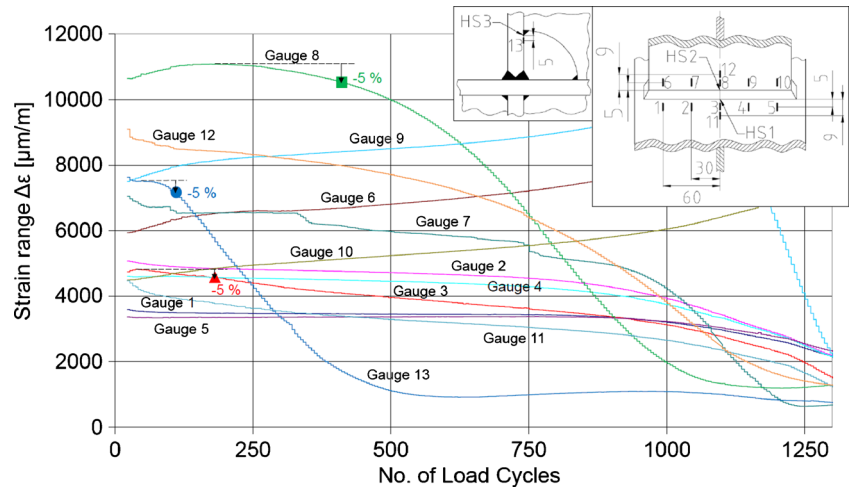


Fig. 7 Strain ranges recorded in model 2

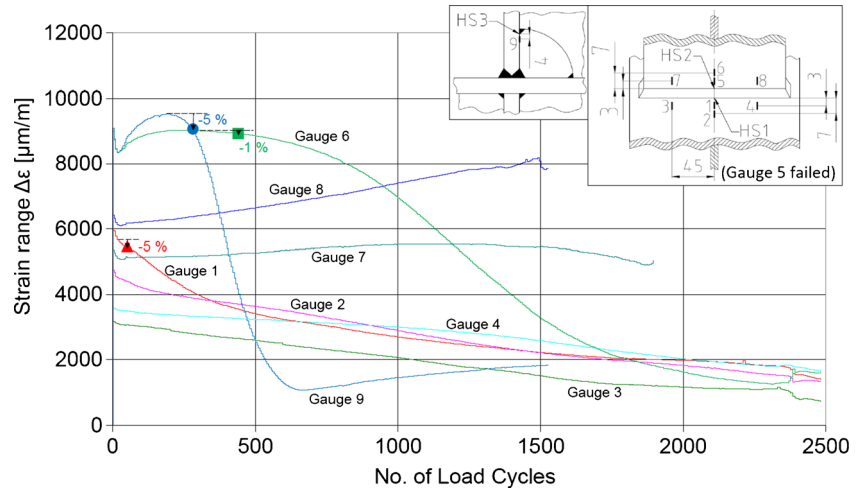


Fig. 8 Strain ranges recorded in model 3

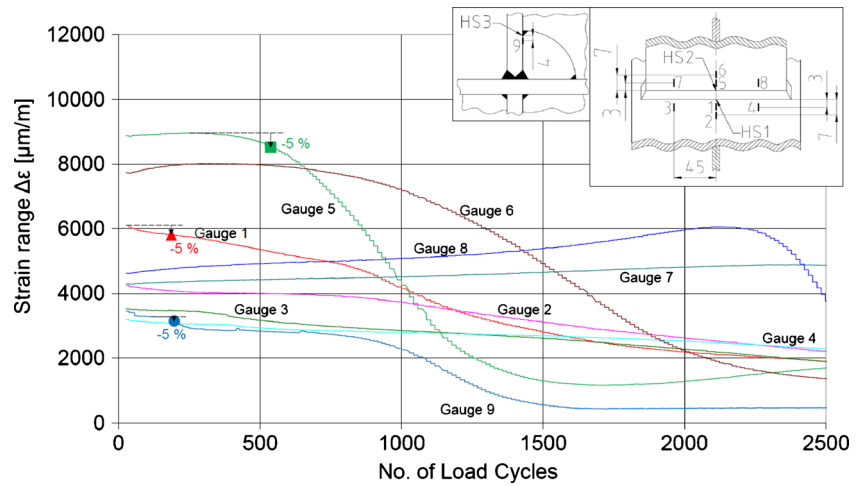
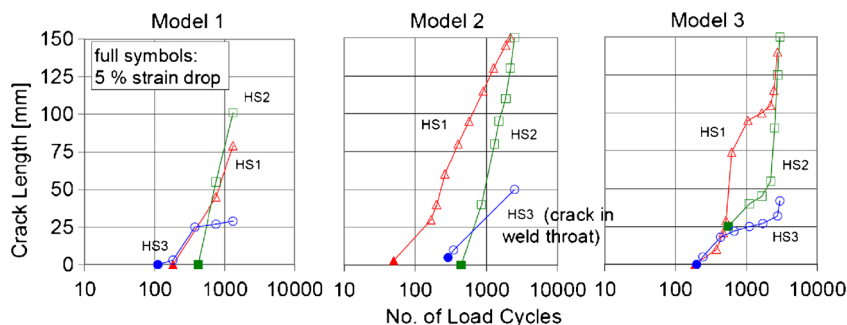


Fig. 9 Observed crack propagation in models 1–3



in front of the welds and great variations in strain range during the tests. The changes are mainly due to the initiation and propagation of cracks resulting in load shedding and redistribution.

A strain drop in a gauge was an indication for crack initiation before it could be detected by optical means. Five percent strain drop was associated with crack initiation, being marked in Figs. 6, 7 and 8 at the signals of the strain gauges closest to the three hot spots HS1–HS3. Unfortunately, strain gauge 5 close to HS2 in model 2 failed. The corresponding strain drop of the next gauge 6 was assumed to be 1 % according to the observations in model 3 (Fig. 8).

It is interesting to note that the first strain drop was observed at HS1 and/or HS3, where rather small and/or shallow cracks appeared, whereas the crack at most highly stressed HS2 occurred later but grew faster and finally dominated the failure (see also Fig. 9). Figure 10 summarizes the crack observations and visually measured crack length which mostly propagated symmetrically to the specimen’s centre line.

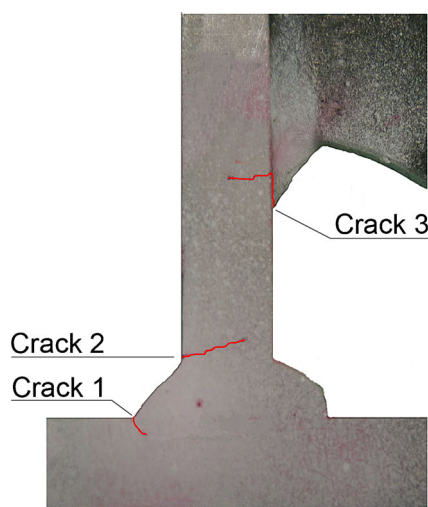


Fig. 10 Position of cracks in central slice of model 1

5 Nonlinear finite element analysis and fatigue assessment

Nonlinear finite element analyses were performed using ANSYS software. A half model was created utilizing the vertical symmetry plane (see Fig. 11). A relatively fine mesh was created using six 20-node solid elements in thickness direction. A refined meshing was used in the way of HS2.

The mild steel used for the test models had an actual yield stress of about 300 MPa. The cyclic material behaviour was assumed to follow the Ramberg-Osgood equation

$$\varepsilon_a = g(\sigma_a) = \frac{\sigma_a}{E} + \left(\frac{\sigma_a}{K'}\right)^{1/n'} \tag{1}$$

giving the relationship between the cyclic stress and strain amplitudes σ_a and ε_a . In the absence of cyclic material data, constants $K'=640$ MPa and $n'=0.113$ were taken from [11], derived from incremental step tests for a comparable steel (see also Fig. 12). A multi-linear material law with kinematic hardening was assumed for the calculations. The same data were simply used for the whole model including welds and HAZ. Previous investigations showed that the effect of over- and undermatching is limited [8].

Figures 13, 14 and 15 show the computed force–strain hysteresis loops together with stabilized measured ones at selected strain gauge locations of models 1, 2 and 3. The agreement is partly good and partly reasonable. The measured displacements and strains are obviously affected by a weaker structure due to pre-deformations and—in case of model 1—by a slightly eccentric loading which, however, should not have influenced the crack initiation in the middle of the model where the highest strains occur. Also, the simplified material law might have affected the results.

The fatigue strength assessment of the weld toe at HS2, where the dominant crack occurred, is based on the local cyclic strain. This was determined in the weld toe which was fictitiously

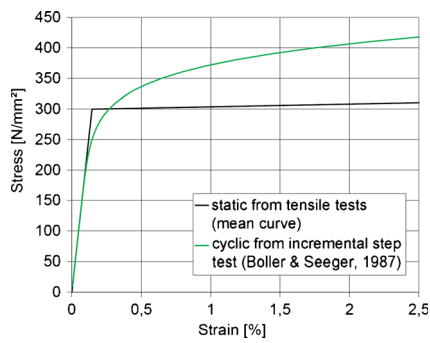


Fig. 11 Static and cyclic material law, the latter taken from [11]

rounded with $r_{ref}=1$ mm according to the effective notch stress approach [4] (see Fig. 16).

$$\Delta\varepsilon_{eff} = \frac{\Delta\bar{\sigma}}{E} + \Delta\bar{\varepsilon}_p \tag{2}$$

$$\Delta\sigma = \sqrt{\frac{1}{2} \left[(\Delta\sigma_x - \Delta\sigma_y)^2 + (\Delta\sigma_y - \Delta\sigma_z)^2 + (\Delta\sigma_z - \Delta\sigma_x)^2 + 6(\Delta\tau_{xy}^2 + \Delta\tau_{yz}^2 + \Delta\tau_{zx}^2) \right]} \tag{3}$$

$$\Delta\varepsilon_p = \frac{1}{3} \sqrt{2 \left[(\Delta\varepsilon_{p,x} - \Delta\varepsilon_{p,y})^2 + (\Delta\varepsilon_{p,y} - \Delta\varepsilon_{p,z})^2 + (\Delta\varepsilon_{p,z} - \Delta\varepsilon_{p,x})^2 + \frac{3}{2} (\Delta\gamma_{p,xy}^2 + \Delta\gamma_{p,yz}^2 + \Delta\gamma_{p,zx}^2) \right]} \tag{4}$$

Where

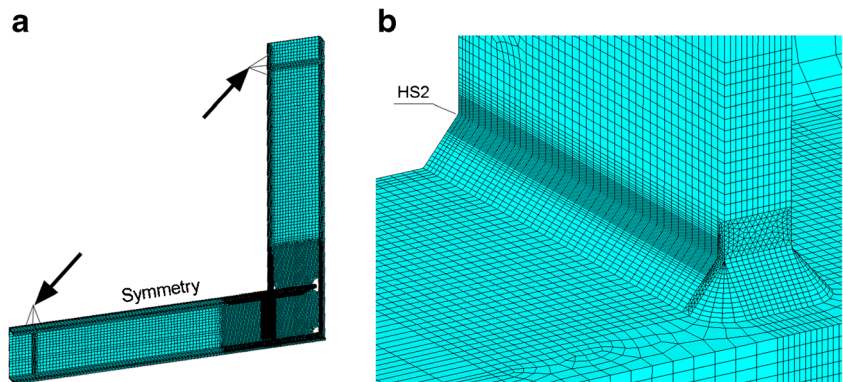
- $\Delta\sigma, \Delta\tau$ Ranges of normal and shear stress
- $\Delta\varepsilon_p, \Delta\gamma_p$ Ranges of plastic normal and shear strain

Table 2 shows the elastic and plastic part as well as the total effective strain range computed for HS2 in the three models. Also shown are the significant plastic strain components. The last column gives the load cycle number at 5 % strain drop in the adjacent strain gauge (1 % strain drop in model 2), i.e. the crack initiation observed in the tests. This crack initiation

criterion differs from the 20 % drop in the load used for the small-scale specimens in [5], which cannot be transferred to large-scale structures like the investigated frame corners.

The lives of the three models are plotted in Fig. 18 in relationship to the computed effective strain range. Also shown are the results including the mean and lower bound lines derived in [5]. The mean curve for these results is slightly conservative with regard to the web frame corner. However, it should be kept in mind that a simplified analysis with only one material model has been performed. It should also be noted

Fig. 12 Finite element model and local mesh in way of HS2



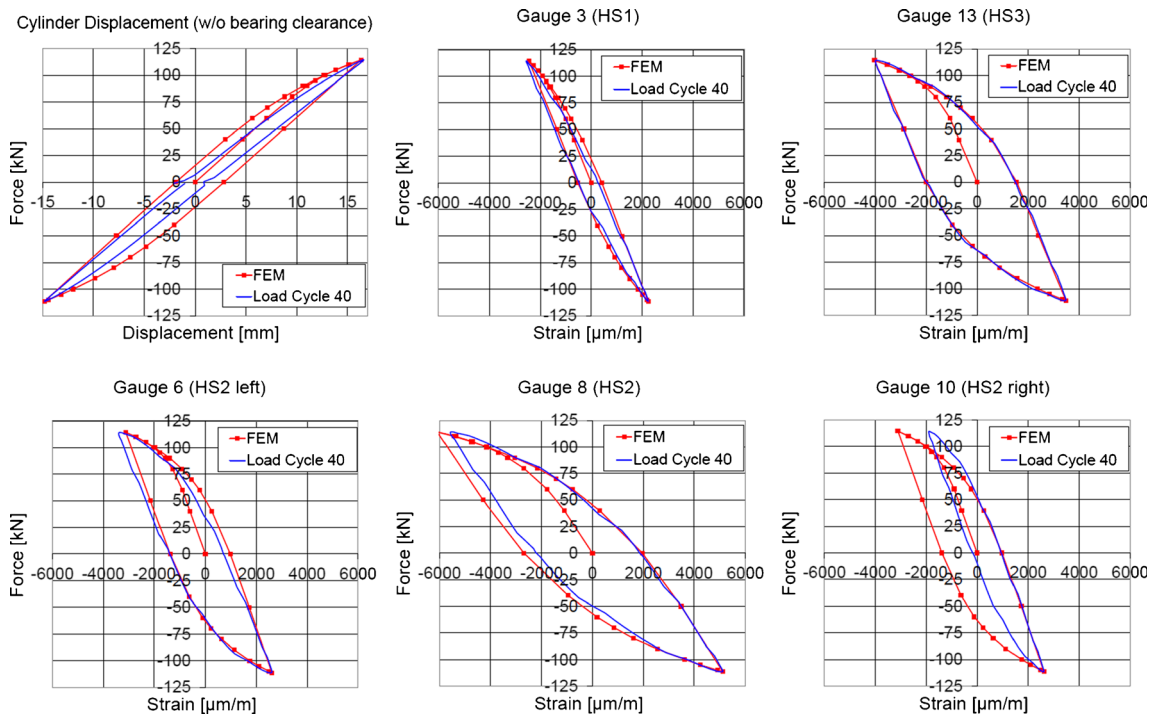


Fig. 13 Computed and measured force–strain hysteresis loops at selected strain gauge locations of model 1 (measured results adjusted to lower reversal point)

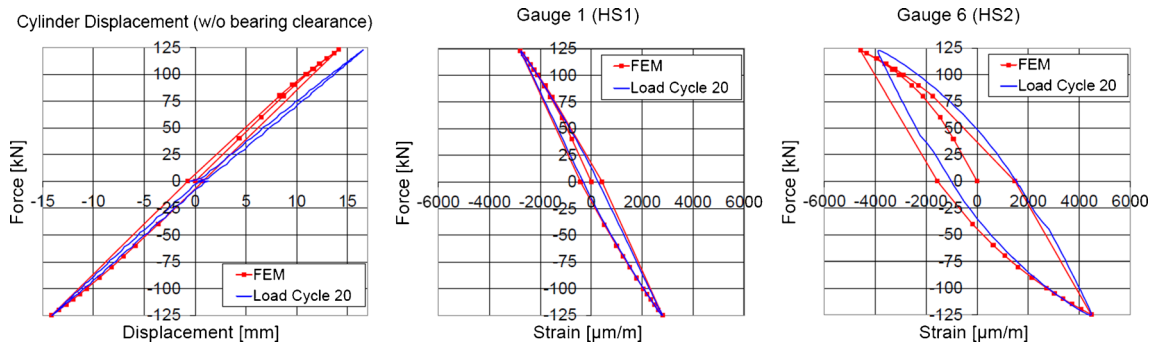


Fig. 14 Computed and measured force–strain hysteresis loops at selected strain gauge locations of model 2 (measured results adjusted to lower reversal point)

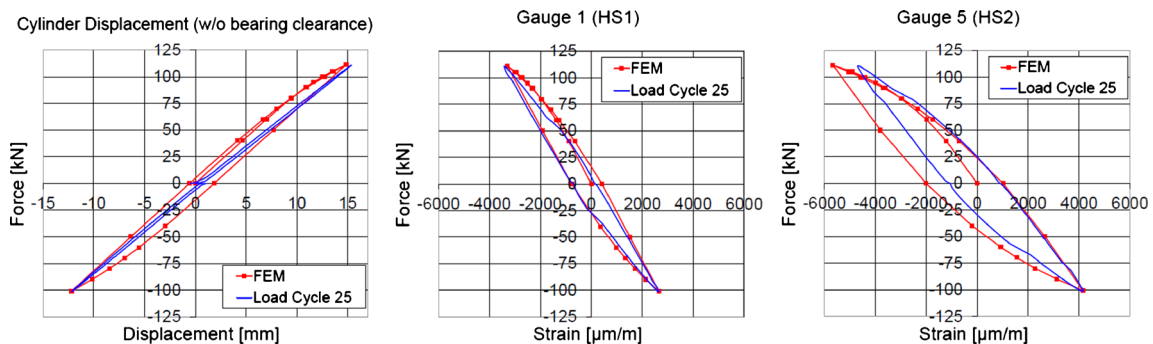


Fig. 15 Computed and measured force–strain hysteresis loops at selected strain gauge locations of model 3 (measured results adjusted to lower reversal point)

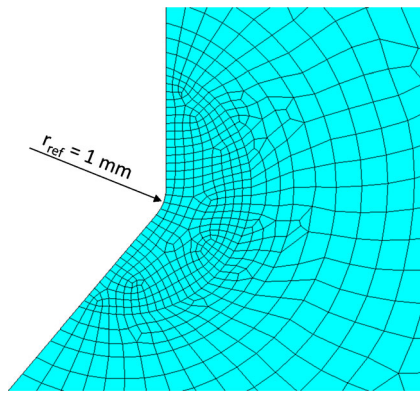


Fig. 16 Refined finite element model with fictitious rounding at HS2

that the lower bound curve is very close to the FAT 200 line, converted into strain, which is recommended in the effective notch stress approach when the von Mises equivalent stress is used.

6 Summary and conclusions

LCF tests were performed for a typical ship structural detail, i.e. a web frame corner with a fatigue-critical cruciform joint. The structure was subjected to rather high cyclic loads creat-

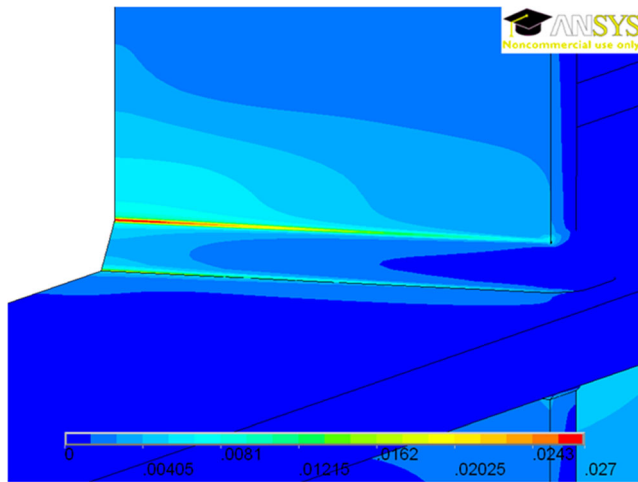


Fig. 17 Computed von Mises strain for model 1 with 114 kN load

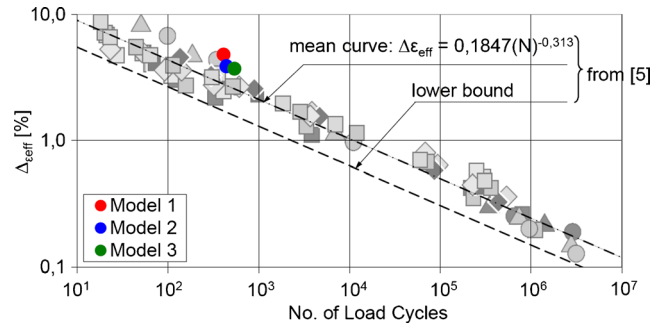


Fig. 18 Crack initiation lives vs. effective strain range of present test models and small-scale specimens from [5]

ing plastic strains at the welded joints and in the adjacent flanges.

From the experimental and associated numerical analyses, the following conclusions are drawn:

- The first small cracks initiated at different weld toes of the frame corner, whereas the dominant crack initiated somewhat later at the location with the largest structural hot spot stress but grew faster and dominated the failure at more than 1,000 cycles.
- Nonlinear finite element analyses showed a stiffer structural behaviour in comparison with the test models. The reason is seen in pre-deformations of the structure not considered in the numerical models.
- Elastic–plastic strains computed and measured at different locations showed partly good and partly fair agreement. Deviations may have been caused by the disregarded pre-deformations mentioned and the fact that a common material model was assumed for the base and weld material.
- In addition, the effective strain range was computed in the weld toe at the dominant crack location rounded by 1 mm as usual in the effective notch stress approach. The crack initiation life predicted with an $S-N$ curve proposed in [5] on the basis of the effective strain range agrees well with the present tests.
- This calls for a simplified fatigue assessment procedure based on the $S-N$ curve of the effective notch stress approach extended into the LCF domain by using the effective notch strain range as fatigue parameter.

Table 2 Computed effective strain range and observed crack initiation life at HS2

Model	Elastic strain range $\Delta\sigma/E$ [%]	Plastic strain component $\Delta\varepsilon_{p,y}$ [%]	Plastic strain component $\Delta\varepsilon_{p,z}$ [%]	Plastic strain component $\Delta\gamma_{p,yz}$ [%]	Plastic strain range $\Delta\varepsilon_p$ [%]	Effective strain range $\Delta\varepsilon_{eff}$ [%]	Load cycles until crack initiation
1	0.4	2.8	3.1	4.8	4.4	4.8	410
2	0.4	2.6	2.5	3.2	3.5	3.9	440
3	0.4	2.1	2.4	3.5	3.3	3.7	540

The early crack initiation observed at the other weld toes leading to less dominant cracks requires further investigations.

References

1. Fricke W, Paetzold H (1987) Application of the cyclic strain approach to the fatigue failure of ship structural details. *J Ship Res* 31:177–185
2. Radaj D, Sonsino CM, Fricke W (2006) Fatigue assessment of welded joints by local approaches, 2nd edn. Woodhead Publ, Cambridge
3. Urm HS, Yoo IS, Heo JH, Kim SC, Lotsberg I (2004) Low cycle fatigue strength assessment of ship structures, Proc. of 9th Int. Symp. on Pract. Design of Ships and Floating Struct. (PRADS'2004), Schiffbautech. Ges., Seehafen Verlag, Hamburg
4. Hobbacher A (2009) Recommendations for fatigue design of welded joints and components, IIW doc.1823-07, Welding Research Council Bulletin 520, Welding Research Council, New York
5. Saiprasertkit K, Hanji T, Miki C (2012) Fatigue strength assessment of load carrying cruciform joints in low and high cycle fatigue region based on effective notch stress approach. *Int J Fatigue* 40:120–128
6. Saiprasertkit K (2014) Fatigue assessment of load carrying cruciform joints in low and high cycle fatigue region based on effective notch concept, IIW-Doc. XIII-2456-13, proposed for publication in *Welding in the World*
7. Hanji T, Miki C, Saiprasertkit K (2012) Low- and high-cycle fatigue behavior of load-carrying cruciform joints containing incomplete penetration and strength mismatch. *Weld World* 56:133–146
8. Tateishi K, Hanji T, Chen T (2007) Low cycle fatigue assessment for welded joints based on local strain approach, IIW-Doc. XIII-2160-07, International Institute of Welding, Paris
9. Tateishi K, Hanji T, Minami K (2007) A prediction model for extremely low cycle fatigue strength of structural steel. *Int J Fatigue* 29:887–896
10. Fricke W, von Lilienfeld-Toal A, Paetzold H (2012) Fatigue strength investigations of welded details of stiffened plate structures in steel ships. *Int J Fatigue* 34:17–26
11. Boller C, Seeger T (1987) Materials data for cyclic loading, part a: unalloyed steels. Elsevier, Amsterdam